Key Engineering Materials
ISSN: 1662-9795, Vol. 734, pp 37-48
doi:10.4028/www.scientific.net/KEM.734.37

Submitted: 2016-09-06
Revised: 2016-12-12
Accepted: 2017-01-17
Online: 2017-04-20

The High Temperature Creep Properties of a Thermally Sprayed CoNiCrAlY Coating via Small Punch Creep Testing

G.A.Jackson[1, a], H.Chen[2, b], W. Sun[1, c *], D.G. McCartney[1, d]

[1]Faculty of Engineering, University of Nottingham, University Park, Nottingham, NG7 2RD, UK

[2]Faculty of Science and Engineering, University of Nottingham Ningbo China, Ningbo 315100, China

[a*] George.Jackson@nottingham.ac.uk, [b] Hao.Chen@nottingham.edu.cn,
[c *] W.Sun@nottingham.ac.uk, [d] Graham.McCartney@nottingham.ac.uk

Keywords: Small Punch Creep Testing, CoNiCrAlY, MCrAlY, HVOF, Creep, Mechanical properties.

Abstract. Thermal barrier coatings (TBC's) protect superalloy components from excessively high temperatures in gas turbines. TBC's comprise of a ceramic top coat, a metallic bond coat and a thermally grown oxide (TGO). The creep behaviour of the MCrAlY bond coat, which is sensitive to the composition and the method of deposition, has a significant effect on the life of the TBC. High velocity oxy-fuel (HVOF) thermal spraying is a popular deposition method for MCrAlY bond coats however the creep properties of HVOF MCrAlY coatings are not well documented. The creep behaviour of a HVOF thermally sprayed CoNiCrAlY coating has been determined by small punch creep (SPC) testing. Tests were conducted between an equivalent uniaxial stress range of 37-80 MPa at 750 °C on two different SPC rigs and between 30-49 MPa at 850 °C on a single SPC rig. The measured steady-state creep deformation rates at 750 °C were consistent across the two rigs. A comparison with previous work demonstrated that the creep behaviour of HVOF CoNiCrAlY coatings is not sensitive to the manufacturing variability associated with HVOF thermal spraying. The CoNiCrAlY coating exhibited typical SPC deformation at 750 °C. At 850 °C the CoNiCrAlY coating showed significantly different creep behaviour which could be attributed to the onset of superplasticity.

1. Introduction

Thermal barrier coating (TBC's) systems are widely used in gas turbines to protect turbine blades from oxidation and high temperature corrosion. The need to continuously increase the turbine inlet temperature in order to improve efficiency requires the continuous development of such coating systems. TBC's typically consist of a Y_2O_3 stabilised ZrO_2 ceramic top coat, an MCrAlY bond coat, where M = Ni, Co or NiCo and a thermally grown oxide (TGO). The MCrAlY bond coat provides oxidation and corrosion resistance through the TGO which is typically an alumina scale [1-4]. Maintaining the integrity of the bond coat is crucial to ensuring the TBC operates reliably. Of particular importance is the creep performance of the MCrAlY bond coat [2] and it has been shown that creep resistant bond coats improve TBC thermal cycle life [5]. MCrAlY bond coats typically consist of fcc Ni(Co)-γ-phase, bcc B2 NiAl-β-phase, ordered $Ni_3(Al,Ti)$ γ' phase and CrCo σ phase [3,6-12]. The microstructure of MCrAlY bond coats can be controlled through careful selection of the alloy composition which allows, in theory, careful control of the mechanical properties, however the mechanical properties of MCrAlY bond coats are also affected by the method of deposition [13]. The creep behaviour of MCrAlY coatings is also dependent upon the composition [14] and the volume fractions of oxide dispersions [15] which means there is little consistent data for any single MCrAlY alloy. Therefore, in order to develop a more comprehensive understanding of the mechanical properties of MCrAlY coatings, in particular the creep performance of MCrAlY coatings, it is necessary to obtain consistent data for MCrAlY coatings manufactured by a single deposition method. High velocity oxy-fuel thermal spraying (HVOF) is a low cost and a widely used deposition method for MCrAlY coatings [13,16-17]. Recently, small punch creep (SPC)

testing has been validated as an effective method for determining the creep properties of HVOF MCrAlY coatings at 750 °C by Chen et al. [6]. The current work aims to develop the work done by Chen et al. by investigating the creep properties of a HVOF CoNiCrAlY coating at 750 and 850 °C. A custom built rig was designed for SPC testing at 850 °C and is compared to the rig used by Chen et al. [6], which has been shown to provide consistent creep data for HVOF CoNiCrAlY alloys at 750 °C. A comparison is drawn between the current work and Chen et al. to determine whether the variability associated with HVOF thermal spraying has a significant effect on the creep performance of HVOF CoNiCrAlY coatings.

2. Experimental Methods

2.1. Materials, HVOF Thermal Spraying and Heat Treatment. Free standing coatings were manufactured by high-velocity oxy-fuel (HVOF) thermal spraying using a commercially available powder known as Praxair CO-210-24 with the following nominal composition: Co-31.7Ni-20.8Cr-8.1Al-0.5Y (wt.%). The powder had a size range of -45+20 μm with a chemically analysed oxygen content of 0.037 wt.% O. The powders were sprayed onto mild steel substrates of dimension 60 × 24 × 1.8 mm using a Met Jet III thermal spray gun to a thickness of approximately 600 μm. The spraying parameters are detailed elsewhere [3]. The coatings were then detached from the substrates by bending around a mandrel. The mild steel substrates were not grit blasted to aid debonding post spraying. Vacuum heat treatment was carried out on free-standing coatings at 1100 °C for two hours in an Elite Thermal Systems TVH12 vacuum tube furnace held at approximately 10^{-9} bar followed by furnace cooling over a period of 6 hours. This heat treatment was carried out in order to approximately replicate the initial heat treatment given to bond coats during the manufacture of thermal barrier coatings. This type of heat treatment has been shown to reduce the porosity within samples and allow the precipitation of secondary phases [3,6]. Discs of 8 mm diameter were cut from heat treated coatings via electric discharge machining and ground to a thickness of 0.4 mm on 1200 grade silicon carbide paper. The final thickness was controlled to within ± 5 μm as measured by digital micrometer and both surfaces had the same finely ground surface finish.

2.2 Microstructural Characterisation. Cross sections of the coating following heat treatment and small punch creep (SPC) testing were mounted, ground and polished to a 1 μm finish. Scanning electron microscopy was carried out using a FEI XL30 scanning electron microscope (SEM) equipped with an Oxford Instrument Link ISIS-3000 energy dispersive X-ray analysis (EDX) detector. Back-scattered electrons (BSE) were used to form images of the coating microstructure in order to measure the volume fraction of the different phases within each coating. EDX was utilised to aid phase identification through chemical microanalysis. Image analysis was carried out using the ImageJ and Gimp 2.0 software packages. The volume fractions stated are the average of the four measurements. Electron back-scatter diffraction (EBSD) was carried out on a Zeiss 1530 VP field emission gun scanning electron microscope (Carl Zeiss, Inc., Maple Grove, MN) with an EDAX Pegasus combined electron backscatter diffraction system (EDAX, Mahwah, NJ, USA). Grain orientation maps and phase maps were recorded at a specimen tilt angle of 70 ° with an accelerating voltage of 20 kV and a beam current of 26 nA over an area of 50 μm × 50 μm at a step size of 0.1 μm. Samples for EBSD required a further stage of chemical/mechanical polishing using colloidal silica to achieve a surface finish of 0.02 μm with minimal surface deformation.

2.3 Small Punch Tensile Testing. Constant load small punch creep (SPC) tests were carried out across two separate SPC rigs, referred to as rig 1 and rig 2. Rig 1 is a custom built dead-load system which has been used previously for SPC testing of the current material and is detailed elsewhere [6].

Rig 2 is a new custom built SPC rig installed on a Tinius Olsen H5KS single column materials testing machine. A schematic of the rig is shown in Fig.1 The load is applied via a 2.5 kN load cell and transmitted to the sample through a hemispherical punch head a) of 1 mm radius (R_s = 1 mm). The punch head is aligned through an alignment bush which is removed after alignment is

complete. The sample is clamped by screwing the top nut b) onto the lower die c), which presses a clamping disc d) onto the sample e). Two pins prevent the clamping disc from rotating and causing sliding on the surface of the sample. The displacement was measured by two LDVT's which measure the displacement of the punch head. The samples were heated to temperature prior to the application of a constant load and held at this temperature for the duration of the test. The temperature was monitored by a thermocouple located at f).

3. Calculation of Stress, Strain and Mechanical Properties

3.1 Stress. The load was converted to equivalent uniaxial stress (σ) using Eq. 1 [18]:

$$\frac{P}{\sigma} = 3.33\, K_{SP}\, {a_p}^{-0.2} {R_s}^{1.2} t \tag{1}$$

where a_p is 2 mm, R_s is 1 mm, t is the specimen thickness (0.4 ± 0.005 mm). P is the load in N and K_{SP} is a non-dimensional correction factor used to correlate SPC work with traditional uniaxial testing. K_{SP} is typically between 1.2~1.3 but where uniaxial test data do not exist, as is the case for free standing MCrAlY coatings, it is taken as 1.

3.1 Strain. The displacement (δ) was converted to equivalent uniaxial strain (ε_q) at the punch contact boundary using Eq. 2 which was empirically derived from membrane stretching theory by Li et al. [19]. The minimum steady state strain rate was calculated using a 1/5th moving average.

$$\varepsilon_q = 0.20465\, \delta + 0.12026\, \delta^2 + 0.00950\, \delta^3 \tag{2}$$

3.2 Material Properties. Linear relationships between the equivalent uniaxial stress, the equivalent uniaxial minimum steady-state strain rate and the time to failure can be obtained from the following three equations. These equations are used to describe the material creep behaviour following SPC testing at 750 and 850 °C.

Norton Steady-State Power Law:

$$\dot{\varepsilon}_{min} = B\, \sigma^n \tag{3}$$

Creep Rupture Power Relationship:

$$t_f = \frac{1}{M \sigma^{\chi}} \tag{4}$$

Monkman-Grant Relationship:

$$t_f = K_1 {\dot{\varepsilon}_{min}}^{-m} \tag{5}$$

Where B, n, M, χ, K_1 and m are temperature dependent material properties.

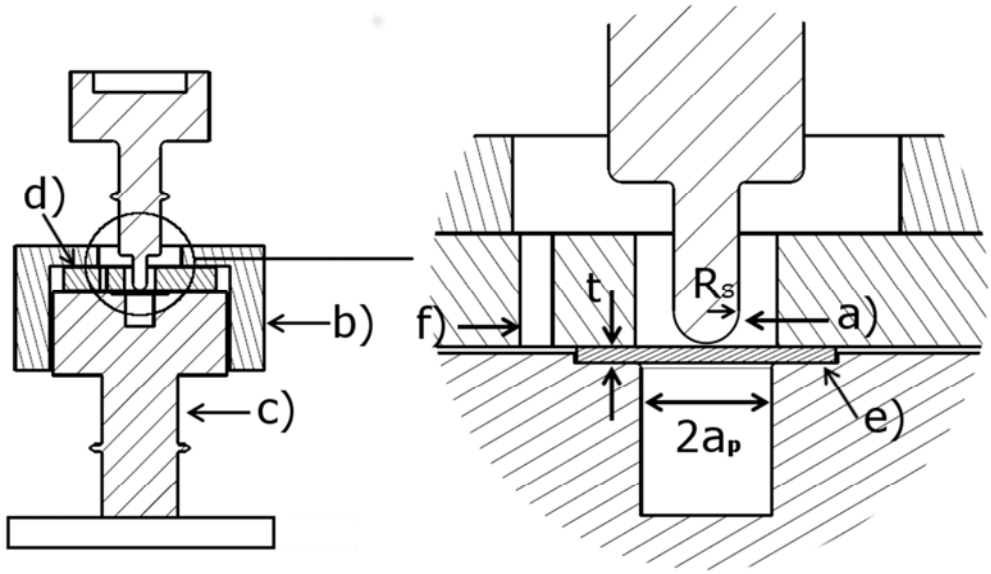

Figure 1. Schematic of custom built small punch creep rig, referred to as rig 2, where R_s = 1.0 mm, a_p = 2.00 mm and t = 0.4 mm in accordance with the CEN workshop agreement [18]. Detailed description is provided in section 2.3.

4. Results and Discussion

4.1 Microstructure of Heat Treated Coatings. Fig. 2a and Fig. 2b are BSE images of the coating at high and low magnification following heat treatment at 1100 °C for 2 hours under vacuum. The material exhibits a dual phase microstructure consisting of a light contrast phase and a dark contrast phase. The light contrast phase is a Ni-based solid solution with a fcc crystal structure normally termed γ-phase. The dark contrast phase is an intermetallic phase with an ordered bcc crystal structure normally referred to as β-phase. The thin, dark elongated regions are oxide stringers of Al_2O_3. The volume fractions of each phase are measured as 68 vol.% γ-phase and 32 vol.% β-phase which agrees with previous characterisation of coatings manufactured from Praxair CO-210-24 [3,6-9]. Fig. 2c and Fig. 2d show a 50 μm × 50 μm region of the coating imaged by EBSD and presented as a grain orientation map and phase map respectively. The grain orientation map selects individual grains and colours them based on grain orientation and it is clear from the random assortment of colours that there is no preferred grain orientation for either phase. The phase map shows the γ-phase as green and the β-phase as red. It is clear that regions of γ-phase can consist of multiple grains whereas the β-phase generally precipitates as single grains. Individual grains range from approximately 1-5 μm in size. The spherical region consisting of larger grains which can be identified in Fig. 2c and Fig. 2d is a powder particle which has, in part, retained the original particle microstructure during HVOF thermal spraying. The areas consisting of very small grains are areas which fully melted during HVOF thermal spraying and recrystallised upon cooling and heat treatment to form a fine grain structure.

4.2 Small Punch Creep Testing at 750 °C.

4.2.1 Evaluation of The New Custom Built SPC rig. The custom built rig detailed in Fig. 1, referred to as rig 2, was manufactured for SPC testing at 850 °C, which is above the maximum operating temperature of rig 1 used previously for SPC testing [6]. Before SPC tests were conducted at 850 °C on rig 2, a comparison study between rig 2 and rig 1 was carried out at 750 °C.

The displacement-time curves obtained from SPC tests at 750 °C are shown in Fig. 3a for rig 1 and Fig. 3b for rig 2. A break has been applied to the x axis in Fig. 3a in order to accommodate the extended loading time at 46 MPa. Each curve exhibits a primary region consisting of a large initial deformation followed by a reduction in the displacement rate, a secondary steady-state region where the displacement rate is approximately constant, and a tertiary region where the displacement rate

accelerates leading to failure. The initial displacement following the application of the load, the overall displacement at failure and the steady-state displacement rate increase as the load is increased. The time to failure decreases as the load is increased. From Fig. 3a and Fig. 3b it can be established that the material exhibits typical creep behavior, as expected from SPC tests, at 750 °C on both rigs.

Fig. 4 shows plots of converted equivalent uniaxial minimum steady-state strain rate as a function of stress (4a), time to failure as a function of stress (4b) and converted equivalent uniaxial minimum steady-state strain rate as a function of time to failure (4c) with all axes plotted on a logarithmic scale. The tests carried out on rigs 1 and 2 are plotted as separate data sets. Linear relationships are drawn between both data sets on each of the separate plots and it is clear that the HVOF CoNiCrAlY coating exhibits consistent creep behaviour across both rigs. From the linear relationships plotted, parameters for the Norton steady-state power law, the creep rupture power law and the Monkman-Grant relationship can be calculated. For the CoNiCrAlY coating at 750 °C, the power law parameters are $B = 4 \times 10^{-20}$ and $n = 7.66$, the creep rupture power law parameters are $M = 6 \times 10^{-13}$ and $\chi = 5.93$, and the Monkman-Grant relationship parameters are $K_1 = 0.003$ and $m = 0.908$. It is clear that the creep performance of the CoNiCrAlY coating is consistent across rig 1 and rig 2, therefore the two rigs can be used interchangeably with a reasonable degree of confidence at 750 °C and rig 2 is suitable for further testing at 850 °C.

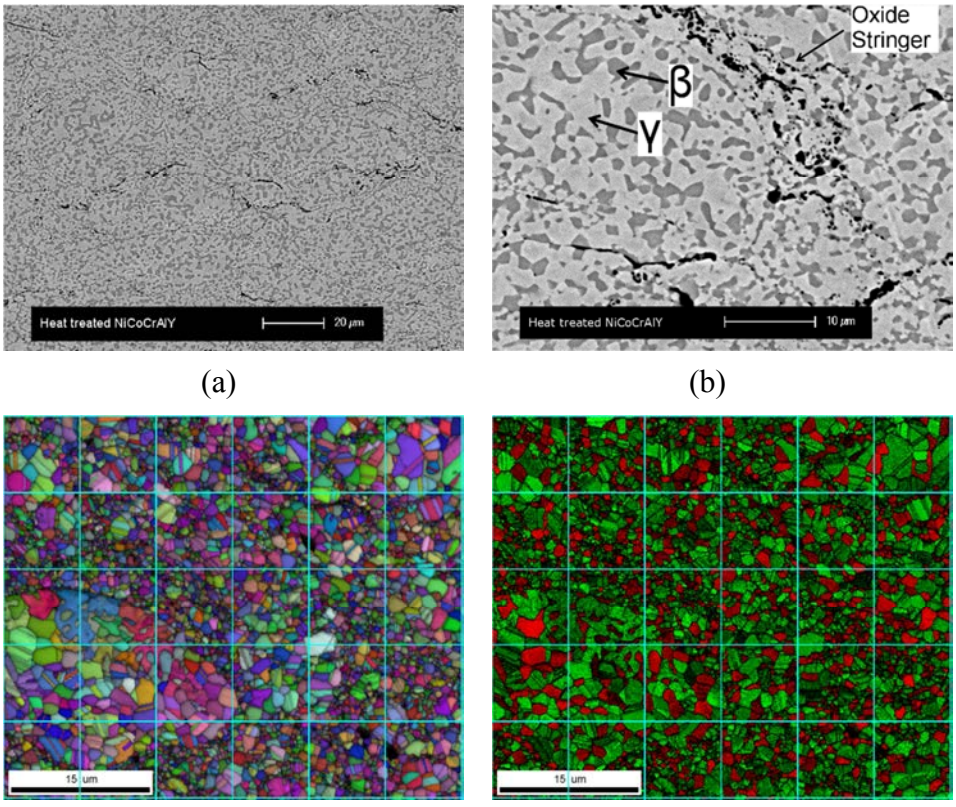

Figure 2. BSE images (top) of the heat treated CoNiCrAlY coating. The light contrast phase is a fcc Ni-γ-phase and the dark contrast phase is a bcc NiAl-β-phase. The dark regions are Al_2O_3 oxides. Images (c) and (d) are EBSD scans presented as a grain orientation map and phase map respectively. The assortment of colours in (c) shows there is no preferred grain orientation for either phase and grains range from approximately 1-5 µm. In the phase map (d) the γ-phase is shown as green and the β-phase is shown as red. The γ-phase matrix consists of multiple grains whereas the β-phase precipitates are generally single grains.

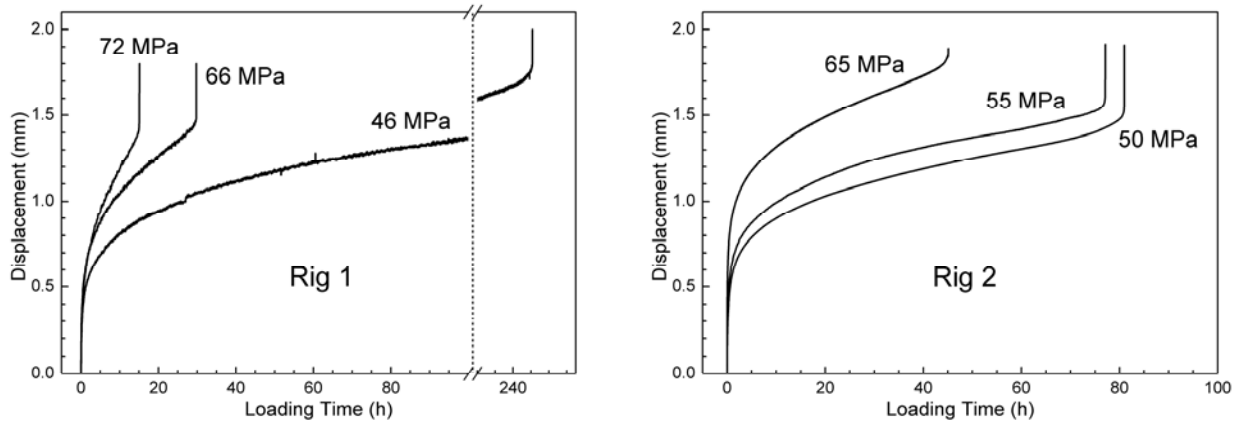

Figure 3. Displacement-time curves for SPC tests conducted at 750 °C on (a) rigs 2 and (b) rig 2. The x axis is shifted in order to fully display the initial displacement region. The CoNiCrAlY coating exhibits typical creep behaviour on both rigs at 750 °C. The steady-state displacement rate increases and the time to failure decreases to as the load is increased.

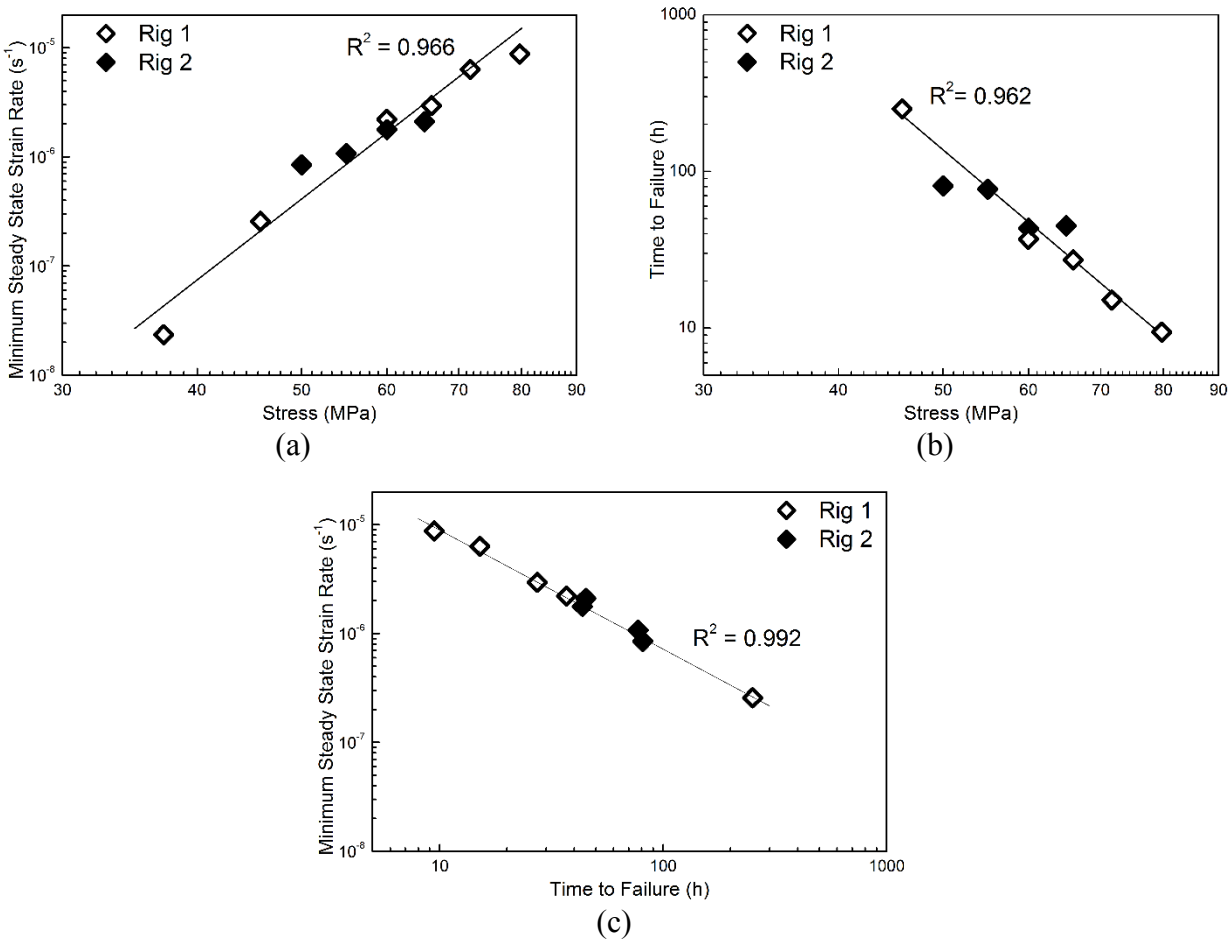

Figure 4. (a) Equivalent uniaxial minimum steady-state strain rate as a function of stress, (b) the time to failure as a function of stress and (c) the equivalent uniaxial minimum steady-state strain rate as a function of time to failure for SPC tests carried out at 750 ˚C on rigs 1 and 2. The CoNiCrAlY coating exhibits consistent creep behaviour across both SPC rigs at 750 ˚C.

4.2.2. Effect of HVOF Variability on the Creep Performance of MCrAlY Coatings. HVOF thermally sprayed coatings deposited at different times often show small variations in microstructure. This is because the microstructure is sensitive to the spray parameters [16,20] which

can fluctuate during spraying. Hence, it is difficult to ensure that HVOF coatings exhibit fully consistent microstructures when sprayed at different times. Of particular importance is the volume of oxide dispersions, which has a significant effect on the creep properties of MCrAlY coatings [15]. In order to establish whether the variability of HVOF thermal spraying has a significant impact on the creep performance of CoNiCrAlY coatings, it is necessary to compare similar HVOF coatings deposited at different times.

Fig. 5 shows the SPC data presented in Fig. 4 superimposed with the SPC data from Chen et al. [6]. The data from the current study is labelled Jackson et al. and the data from the previous study is labelled Chen et al. C1 and C2 were HVOF coatings manufactured from Praxair CO-210-24 deposited at different times using the same spray parameters detailed in [3]. The data from Chen et al. [6] has been recalculated and presented with permission from the authors. Linear relationships are drawn on each of the figures and it is clear that the current data is in good agreement with the previous results. The material properties calculated for the Norton steady-state power law, the creep rupture power law and the Monkman-Grant relationship are presented in Table 1. It is clear that the creep behaviour of similar HVOF CoNiCrAlY coatings, deposited at different times, is consistent at 750 °C.

The equivalent uni-axial minimum steady-state strain rate as a function of stress (Fig. 5a) is typically higher for the Jackson et al. data than for the Chen at al. data. The time to failure is also shorter for a given stress for the Jackson et al. data. This is likely due to a variation in thickness of the specimens used; Chen et al. specimens were 0.43 mm thick and the specimens used in the current work were 0.40 mm thick in order to more accurately represent MCrAlY bond coats used in service which are typically around 0.2 mm thick. This assumption can be considered reasonable as the two HVOF coatings studied by Chen et al. showed very similar material creep behaviour, therefore the difference in the results can be attributed to differences in the studies and not differences in the HVOF CoNiCrAlY creep behaviour.

Table 1. Material properties for the HVOF CoNiCrAlY coatings tested at 750 °C on rigs 1 and 2. The Chen et al. data for HVOF CoNiCrAlY coatings tested at 750 °C on rig 1 [6] has been recalculated with permission from the authors. The material properties calculated at 750 °C are consistent for HVOF CoNiCrAlY coatings deposited during different spray runs.

	Norton power law Eq. 3		Creep rupture relationship Eq. 4		Monkman-Grant relationship Eq. 5	
	B	n	M	χ	K_1	m
Jackson et al. 750 °C	4×10^{-20}	7.66	6×10^{-13}	5.93	0.003	0.908
Chen et al. 750 °C	6×10^{-21}	7.94	9×10^{-14}	6.21	0.0017	0.778

4.3 Small Punch Creep Testing at 850 °C. Small punch creep tests at 850 °C were carried out using only rig 2 as 850 °C is above the maximum operating temperature of rig 1. Fig. 6a shows representative displacement-time curves obtained for SPC tests at 850 °C. The displacement-time curve for one test conducted at 750 °C on rig 1 at 46 MPa is provided as a representative displacement-time curve for the material creep behaviour at 750 °C. The steady-state displacement rate is lower at 850 °C than at 750 °C, even when the load is higher. The time to failure is also significantly higher at 850 °C, the curve obtained at 49 MPa and 850 °C exceeds the time to failure of the sample tested at 46 MPa and 750 °C. No time to failure is shown for the 850 °C tests as no sample was tested to failure at that temperature. Extrapolating the time to failure data at 750 °C, based on the measured minimum steady-strain rates seen at 850 °C, predicted times to failure in excess of 1000 hours which was not feasible in the current work.

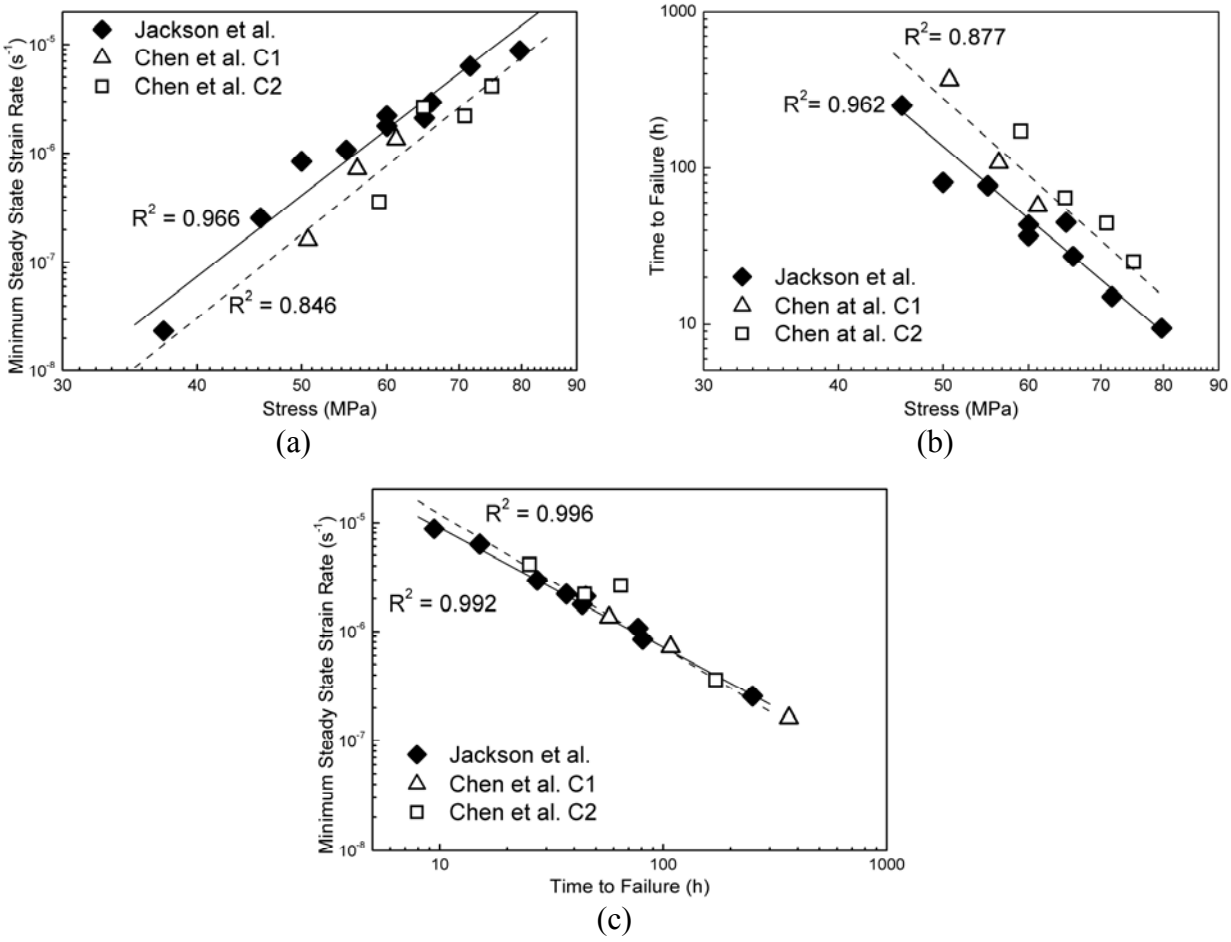

Figure 5. (a) Equivalent uniaxial minimum steady-state strain rate as a function of stress, (b) the time to failure as a function of stress and (c) the equivalent uniaxial minimum steady-state strain rate as a function of time to failure for all SPC tests carried out on rigs 1 and 2 at 750 °C as well as the SPC data obtained by Chen et al. [6]. The creep behaviour of HVOF CoNiCrAlY coatings deposited during different spray runs is reasonably consistent at 750 °C.

Fig. 6b shows the equivalent uniaxial minimum steady-state strain rate as a function of stress for all tests carried out at 750 and 850 °C with both axis plotted on a logarithmic scale. A linear relationship can be drawn for the 850 °C tests and it is clear that the minimum steady-state strain rate increases with the stress, similar to the tests at 750 °C, however the minimum steady-state strain rate is clearly lower at 850 °C than at 750 °C. For a material that follows Fick's law of diffusion an increase in temperature should result in an increase in the strain rate however that is not the observed relationship. The Norton steady-state power law parameters for the CoNiCrAlY coating at 850 °C are $B = 7 \times 10^{-11}$ and $n = 2.03$, compared to $B = 4 \times 10^{-20}$ and $n = 7.66$ at 750 °C (see Table 2). Material parameters for the creep rupture relationship and the Monkman-Grant relationship are not presented as no time to failure was recorded for SPC tests at 850 °C.

In order to understand why the equivalent uniaxial minimum steady-state strain rate is lower at 850 °C compared to 750 °C cross sections of samples tested at each temperature were inspected. Fig. 7 shows cross sections of samples tested at 750 °C and 850 °C for samples that were both stopped prior to failure. Fig. 7a and Fig. 7b show low magnification back-scatter electron (BSE) images of the overall specimen deformation at 750 and 850 °C respectively. At 750 °C there exists an area of maximum thinning indicated by A, the thickness increases away from A towards the centre of the sample and towards the inflection point indicated by B. The thickness of the sample is not uniform between points A and B. The dark regions indicate areas where void cavitation and oxide formation has taken place, at 750 °C the dark regions do not fully extend from point A to point B. This type of sample deformation at 750 °C has been previously reported for SPC testing of

this material [6]. The sample deformation at 850 °C is shown in Fig. 7b and is clearly different to the deformation seen at 750 °C. There is an area of maximum thinning indicated by A, however the thinning is much less significant than at 750 °C and the specimen maintains an approximately constant thickness throughout the deformed region. The dark regions indicating void cavitation and oxide formation extend further from the centre of the sample up to point B. The concentration of voids/oxides indicate the areas of highest creep damage, for a typical SPC sample this occurs on the bottom surface of the sample at the point of maximum thinning [21]. This type of damage accumulation can be observed for the sample at 750 °C in Fig. 7c. At 850 °C there is also significant damage accumulation in the area of maximum thinning as seen in Fig. 7d. The dark region indicated by C is a large crack which has developed in the mid-plane of the sample. The inflection point indicated by B also shows an area of high damage accumulation, which is not observed at 750 °C. It is clear that the damage accumulation and deformation behaviour is significantly different at 850 °C compared to 750 °C. A possible explanation for the difference in creep behaviour is that the CoNiCrAlY coating has become superplastic at 850 °C, which has been shown to affect the creep behaviour of MCrAlY coatings above 850 °C [22]. The effect of superplasticity on the creep behaviour of the CoNiCrAlY coating during SPC testing is not fully understood at this stage and further work is needed to confirm the findings, however the current results show that there is a significant decrease in the observed equivalent uniaxial minimum steady-state strain rate between 30-50 MPa at 850 °C and that the overall creep behaviour and sample deformation at 850 °C is significantly different than at 750 °C.

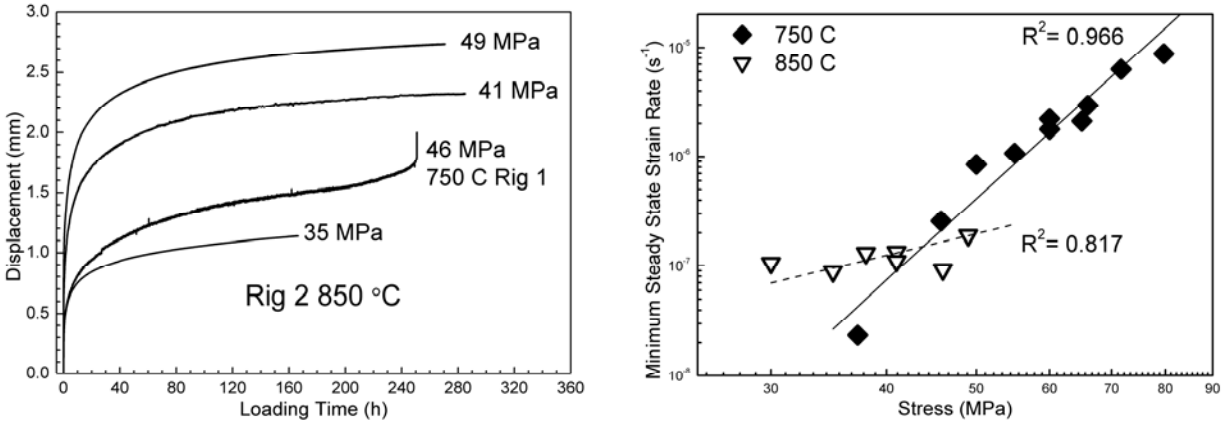

(a) (b)

Figure 6. (a) displacement-time curves for SPC tests carried out on rig 2 at 850 °C. One curve at 750 °C is given as a reference to to SPC tests at 750 °C. The initial displacement is significantly higher at 850 °C compared to 750 °C and the displacement rate is significantly lower. (b) Equivalent uniaxial minimum steady-state strain rate as a function of stress for all SPC tests at 750 and 850 °C. The CoNiCrAlY coating exhibits much lower steady-state strain rates at 850 °C than at 750 °C and exhibits significantly different material properties.

Table 2. Norton steady-state power law parameters for the HVOF CoNiCrAlY coating at 750 and 850 °C showing the distinct change in material behaviour.

	Norton Power law	
	B	*n*
750 °C	4×10^{-20}	7.66
850 °C	7×10^{-11}	2.03

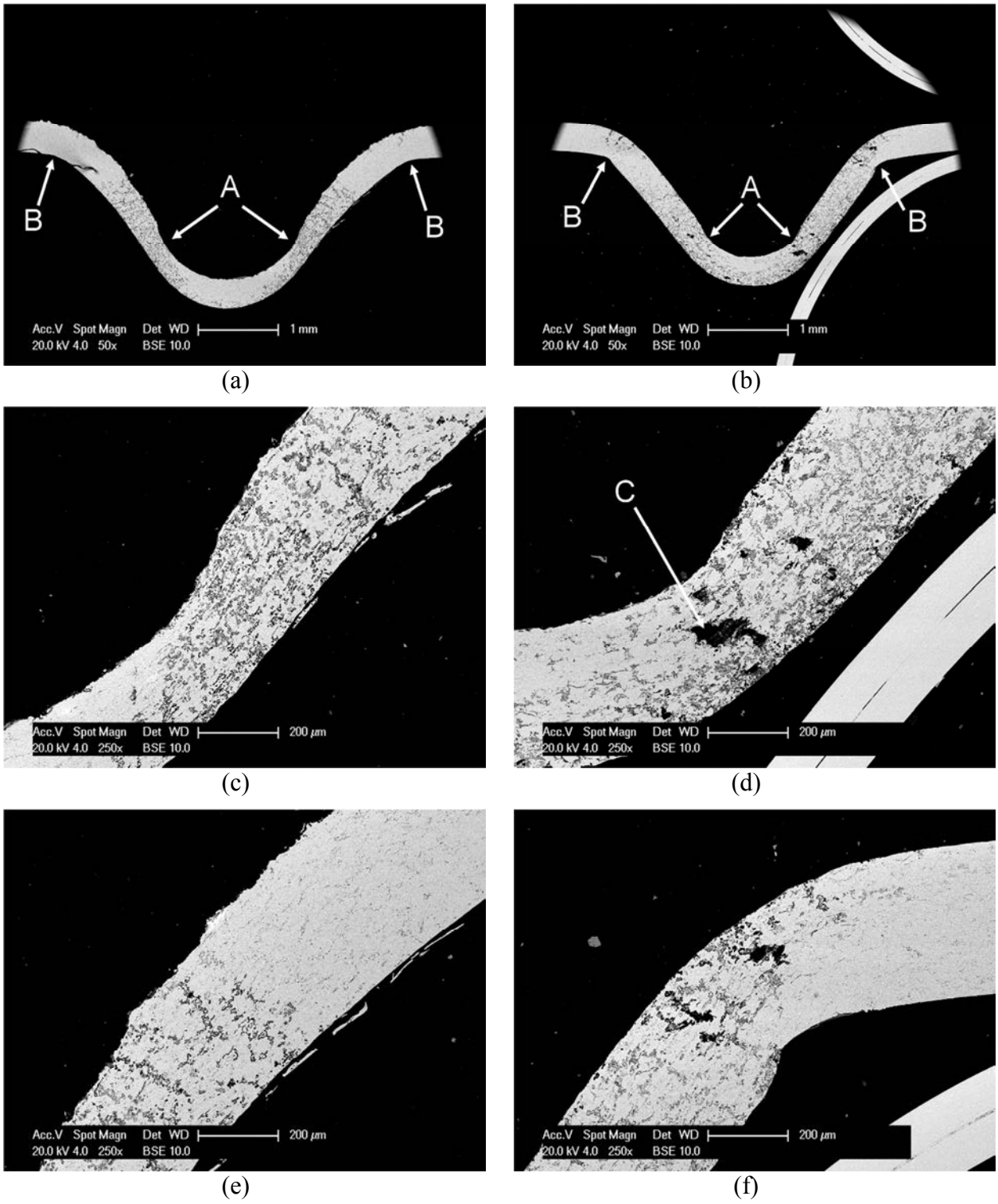

Figure 7. BSE electron images of SPC samples tested at 750 °C (left) and 850 °C (right). At 750 °C the CoNiCrAlY coating exhibits typical SPC deformation. At 850 °C the coating shows uniform thinning throughout the deformed region of the sample and much more damage accumulation at the point of inflection (B). The CoNiCrAlY coating clearly exhibits different creep behaviour at 850 °C compared to 750 °C.

5. Conclusions

- The heat treated HVOF CoNiCrAlY coating exhibited a dual phase microstructure consisting of 68 vol.% fcc γ-phase and 32 vol.% bcc β-phase. The EBSD grain orientation map showed that there was no preferred grain orientation and that the grains ranged in size from approximately 1-5 μm.
- Consistent creep performance was observed on rigs 1 and 2 which validated the new custom built rig for further SPC testing.
- The current work was consistent with previous SPC testing of similar coatings [6]. It can be established that the variability of HVOF thermal spraying does not significantly affect the creep properties of HVOF sprayed CoNiCrAlY coatings.
- At 850 °C the HVOF CoNiCrAlY coating showed significantly lower creep rates than at 750 °C. Typical sample deformation was observed for SPC samples at 750 °C. At 850 °C the specimen deformation and creep damage accumulation was significantly different and had not been previously observed for the CoNiCrAlY coating. It is thought that the change in creep behaviour observed at 850 °C can be attributed to the onset of superplasticity, which has been shown to affect the creep behaviour of MCrAlY coatings above 850 °C [22]. A more detailed investigation is need to further understand the deformation mode and to confirm the change in creep behaviour observed at 850 °C.

Acknowledgements

The authors would like to thank the University of Nottingham for the continued financial support towards this work and would like to acknowledge Shane Maskill for his continued technical support. We would also like to thank Geoff West at the University of Loughborough for his assistance in EBSD imaging and the Armourers and Brasiers Gauntlet Trust for their sponsorship in attending this conference.

References

[1] S. Bose. High Temperature Coatings. Butterworth-Heinemann, 2007.
[2] A.G. Evans, D.R. Mumm, J.W. Hutchinson, G.H. Meier, and F.S. Pettit. Mechanism controlling the durability of thermal barrier coatings. Progress in Materials Science, 46, 2001.
[3] S. Saeidi, Voisey K.T., and D.G. McCartney. The effect of heat treatment and the oxidation behaviour of HVOF and VPS CoNiCrAlY coatings. J. Thermal Spray Tech., 18:209–216, 2009.
[4] Y.H. Sohn, J.H. Kim, E.H. Jordan, and M. Gell. Thermal cycling of EB-PVD/MCrAlY thermal barrier coatings: I. microstructural development and spallation mechanisms. Surface and Coatings Technology, 146-147:70–78, 2001.
[5] D.J. Wortman, E.C. Duderstadt, and W.A. Nelson. Bond coat development for thermal barrier coatings. Journal of Engineering for Gas Turbines and Power, 112:527–530, 1990.
[6] H. Chen, T.H. Hyde, Voisey K.T., and D.G. McCartney. Application of small punch creep testing to a thermally sprayed CoNiCrAlY bond coat. Materials Science and Engineering: A, 585:205–213, 2013.
[7] T. Mori, S. Kuroda, M. Hideyuki, H. Katanoda, Y. Sakamoto, and S. Newman. Effect of initial oxidation on beta phase depletion and oxidation of CoNiCrAlY bond coat coatings fabricated by warm spray and HVOF processes. Surface and Coatings Technology, 221:59–69, 2013.
[8] K. Yuan, R. Eriksson, R.L. Peng, X.H. Li, S. Johansson, and Y.D. Wang. MCrAlY coating design based on oxidation-diffusion modelling. part i: Microstructural evolution. Surface and Coatings Technology, 254:79–96, 2014.
[9] A. Gil, D. Naumenko, R. Vassen, J. Toscano, M. Subanovic, L. Singheiser, and W.J. Quadakkers. Y-rich oxide distribution in plasma sprayed MCrAlY- coatings studied by SEM with a cathodoluminescence detector and raman spectroscopy. Surface and Coatings Technology, 204:531–538, 2009.

[10] D.R.G. Achar, R. Munoz-Arroyo, L. Singheiser, and W.J. Quadakkers. Modelling of phase equilibria in MCrAlY coating systems. Surface and Coatings Technology, 187:272–283, 2004.
[11] J. Toscano, A. Gil, T. Huttel, E. Wessel, D. Naumenko, L. Singheiser, and W.J. Quadakkers. Temperature dependence of phase relationships in different types of MCrAlY - coatings. Surface and Coatings Technology, 202:603–607, 2007.
[12] C. Costa, E. Barbareschi, P. Guarnone, and G. Borzone. Phase evolution in an MCrAlY coating during high temperature exposure. Journal of Mining and Metallurgy, Section B: Metallurgy, 48(3):359–365, 2012.
[13] S. Saeidi, Voisey K.T., and D.G. McCartney. Mechanical properties and microstructure of VPS and HVOF CoNiCrAlY coatings. Thermal Spray Technology, 20(6):1231–1243, 2011.
[14] J.A. Thompson, Y.C. Tsui, R.C. Reed, D.S. Rickerby, and T.W. Clyne. Creep of plasma spraying CoNiCrAlY and NiCrAlY bond coats and it's effect on residual stresses during thermal cycling of thermal barrier coating systems. In J. Nicholls, editor, High Temperature Surface Engineering, pages 199–212. IOM, Maney, 2000.
[15] T.A. Taylor and D.F. Bettridge. Development of alloyed and dispersion-strengthened MCrAlY coatings. Surface and Coatings Technology, 86-87:9–14, 1996.
[16] E. Lugsheider, C. Herbst, and L. Zhao. Parameter studies on high-velocity oxy-fuel spraying of MCrAlY coatings. Surface and Coatings Technology, 108-109:16–23, 1998.
[17] V. Higuera, F.J. Belzunce, and J. Riba. Influence of the thermal-spray procedure on the properties of a CoNiCrAlY coating. Surface and Coatings Technology, 200:5550–5556, 2006.
[18] CEN CWA 15627 Worskshop Agreement: Small punch test method for metallic materials. European Committee for Standardization, Brussels, December 2006.
[19] Y. Li, M. Sun, and C. Zhang. Practical approach to determine creep properties from small punch test. In M. Karel, R. Hurst, and W. Sun, editors, 2nd International Conference SSTT Determination of Mechanical Properties of Materials by Small Punch and Other Miniature Testing Techniques, pages 47–63. Ocelot, 2012.
[20] L. Zhao, M. Parco, and E. Lugsheider. High velocity oxy-fuel thermal spraying of a NiCoCrAlY
alloy. Surface and Coatings Technology, 179:272–278, 2004.
[21] J.P. Rouse, F. Cortellino, W. Sun, T.H. Hyde, and J. Shingledecker. Small punch creep testing: review on modelling and data interpretation. Materials Science and Technology, 29(11):1328–1345, 2013.
[22] M.G. Hesbur and R.V. Miner. High temperature tensile and creep behaviour of low pressure plasma-sprayed NiCoCrAlY coating alloy. Materials Science and Engineering, 83:239–245, 1986.